Absorbing boundary conditions for anisotropic elastodynamic media

Hélène Barucq, Lionel Boillot, Henri Calandra, Julien Diaz

ACOUSTICS 2012

Absorbing boundary conditions for anisotropic elastodynamic media

H. Barucq[a], L. Boillot[a], H. Calandra[b] and J. Diaz[a]

[a]INRIA, Universite de Pau, Avenue de l'Universite, 64013 Pau, France
[b]Total, Centre Scientifique et Technique Jean Féger, Avenue Larribau, 64018 Pau, France
helene.barucq@inria.fr

Reverse Time Migration (RTM) technique produces images of the subsurface thanks to the propagation of waves. We focus on Tilted Transverse Isotropic (TTI) media which come into the category of anisotropic media. The finite element solution of this problem requires the design of efficient boundary conditions that are able to attenuate possible artificial reflected waves generated by the boundaries of the computational domain. In the case of elastic waves, Perfectly Matched Layers (PMLs) are widely used. However, instabilities may appear in the layers, either due to the numerical discretization or to the continuous PML problem as for the TTI case. But RTM is based on the cross-correlation of the source propagation. Thus artificial reflected waves should not be taken into account by the imaging condition. In this work, we propose to consider an Absorbing Boundary Condition (ABC) and to study how it performs in the RTM framework. Moreover, it is easily included in a high-order Discontinuous Galerkin Method (DGM) formulation. Herein we limit our study to a low-order ABC and numerical experiments with a DGM scheme illustrate the good performance of this condition, which is new for the TTI case.

1 Introduction

Reverse Time Migration (RTM) is one of the most widely used technique of Seismic Imaging. However, it requires a lot of computational resources because it is based on many successive solutions of the wave equation. Since geophysical domains are either infinite or very large compared to the wavelengths of the problem, it is necessary to reduce the computational domain to a box, focusing on the simulation of the wave propagation between a source and its receivers.

When considering acoustic or elastic isotropic media, this can be done by applying an Absorbing Boundary Condition (ABC, [5, 6]) at the boundary of the computational domain or by surrounding the computational domain by a Perfectly Matched Layer (PML, [2, 3]). Low-order ABCs are easy to implement but they are not very accurate since they generate spurious reflections. Nevertheless, in a RTM framework, where all the solutions are cross-correlated, these reflections do not really impact on the accuracy of the final image. High-order ABCs are much more accurate, but they induce a severe increase of the computational costs and their implementation can be complicated. PMLs are often preferred to ABCs. Actually they combine the advantages of high- and low-order ABCs: they are relatively easy to implement, they do not generate spurious reflections and their computational costs are less than those of high-order ABCs.

Yet, PMLs are known to be unstable for different classes of anisotropic media [1] and in particular for Tilted Transverse Isotropic media which are of high interest for geophysicists, see [9]. In this case, PMLs induce exponentially increasing modes which completely pollute the solution. It is therefore interesting to develop appropriate ABCs. The aim of this paper is to present a new low-order ABC for TTI media, which is as accurate as the low-order ABCs for isotropic media. Moreover, this ABC can be easily included in Discontinuous Galerkin formulations, which are becoming more and more popular among the geophysical community.

The outline of the paper is as follows. In Section 2, we recall the system of equations to be solved in TTI media. Then, in Section 3, we recall the Discontinuous Galerkin formulation we are using. Section 4 is devoted to the construction of an ABC for Vertical Transverse Isotropic (VTI) media, which are a particular class of TTI media, where the anisotropy axis is the vertical axis of the computaional domain. This is a necessary step prior to the construction of ABCs for TTI media. Indeed, the ABC we propose is easily deduced for the VTI-ABC and its construction is explained in Section 5. Numerical results illustrate then the performance of the new ABC.

2 Anisotropic elastodynamics

Let Ω be an open bounded domain of $\mathbb{R}^2$, its boundary is denoted by $\Gamma = \partial\Omega$ with the exterior normal $\mathbf{n}_\Gamma$. Let $\mathbf{x} = (x, z) \in \Omega$ and $t \in [0, T]$ be the space and time variables, the velocity-stress formulation[1] of the elastic wave equation is

$$\begin{cases} \rho(\mathbf{x})\partial_t v(\mathbf{x}, t) &= \nabla.\underline{\underline{\sigma}}(\mathbf{x}, t) \\ \partial_t \underline{\underline{\sigma}}(\mathbf{x}, t) &= \underline{\underline{C}}(\mathbf{x}) : \underline{\underline{\epsilon}}(v(\mathbf{x}, t)) \end{cases} \tag{1}$$

with $\rho > 0$ the volumic mass, $v \in H^1(\Omega \times [0, T])$ the unknown velocity field, $\underline{\underline{\sigma}}$ such that $\left\{\sigma_{ij} \in H^1(\Omega \times [0, T])\ \forall i, j \in \{x, z\}\right\}$ the stress tensor, $\underline{\underline{C}}$ the stiffness tensor (elasticity coefficients) and $\underline{\underline{\epsilon}}(v) = \frac{1}{2}(\boldsymbol{\nabla} v + (\boldsymbol{\nabla} v)^T)$ the strain tensor (infinitesimal strain theory) with ∇ the divergence and $\boldsymbol{\nabla}$ the gradient.

In geophysics, Earth's crust (geological layers of rocks) is assumed to be locally polar anisotropic, also called transversely isotropic[2]. The difference with full anisotropy lies in the elastic tensor of the medium. This stiffness tensor $\underline{\underline{C}}$ is fourth-rank, i.e. it is composed of elements C_{ijkl} with $i, j, k, l \in \{1, 2\}$ meaning $\{x, z\}$. Since it is symmetric in (i, j) and (k, l), it can be viewed as a matrix in 2D Voigt notation[3],

$$C = \begin{bmatrix} C_{11} & C_{12} & C_{13} \\ C_{12} & C_{22} & C_{23} \\ C_{13} & C_{23} & C_{33} \end{bmatrix}. \tag{2}$$

Wave equation is usually studied in isotropic media to simplify the computations. In these cases, materials are characterized by the two Lamé coefficients λ, μ and

$$C_{11} = \lambda + 2\mu,\ C_{22} = \lambda + 2\mu,\ C_{33} = \mu,\ C_{12} = \lambda.$$

This can be written with the P-waves and S-waves velocities V_p and V_s,

$$C_{11} = \rho V_p^2,\ C_{22} = \rho V_p^2,\ C_{33} = \rho V_s^2,\ C_{12} = \rho(V_p^2 - 2V_s^2).$$

Geophysicists are interested in transversely isotropic media to improve the accuracy of the results in the wave simulation step of the RTM. When the symmetry axis is vertical (resp. horizontal), it is called Vertical (resp. Horizontal)

[1] the velocity-stress formulation is the first-order hyperbolic system of the wave equation defined in Virieux [10] (instead of second-order terms in the displacement-stress formulation)

[2] transversely isotropic material has identical properties along any direction perpendicular to a special one, which is called the symmetry axis

[3] 2D Voigt notation $ij(v)$: $xx(1)$, $zz(2)$, $xz(3)$

Transverse Isotropy (VTI, resp. HTI). When symmetry axis is away from the vertical one, with a measured angle θ, it is called Tilted Transverse Isotropy (TTI). Different behaviours of the wavefronts in TI media are represented in Figure 1.

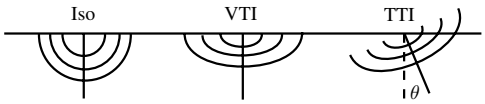

Figure 1: Wavefronts for isotropic and transversely isotropic (vertical and tilted) media

In order to characterize VTI, Thomsen [7] defined three medium parameters: $\varepsilon,\ \delta,\ \gamma$ (the last concerns 3D case only) and the tensor reads as

$$C_{11} = \rho V_p^2(1+2\varepsilon),\ C_{22} = \rho V_p^2,\ C_{33} = \rho V_s^2,$$
$$C_{12} = \rho\left(\sqrt{(V_p^2 - V_s^2)^2 + 2\delta V_p^2(V_p^2 - V_s^2)} - V_s^2\right).$$

TTI media are characterized by the VTI coefficients and the angle θ. The TTI 2D tensor is computed from the VTI one by the rotation

$$\underline{\underline{C}}^{TTI}_{ijkl} = \sum_{p=1}^{2}\sum_{q=1}^{2}\sum_{r=1}^{2}\sum_{s=1}^{2} R_{pi}R_{qj}R_{rk}R_{sl}\underline{\underline{C}}^{VTI}_{pqrs},\ \forall\{i,j,k,l\} \quad (3)$$

with

$$R = \begin{pmatrix} \cos\theta & -\sin\theta \\ \sin\theta & \cos\theta \end{pmatrix}.$$

In this case, the elastic tensor becomes fully non-zero (but still symmetric).

3 Discontinuous Galerkin Method

Let Ω_h be a polygonal mesh (composed of triangles K in 2D) forming a partition of Ω. Contrary to FEM, the principle of DGM consists in approximating the functions v and $\underline{\sigma}$ by discontinuous functions v_h and $\underline{\sigma}_h$ such that $\left\{v_h, \underline{\sigma}_h\right\} \in L^2(\Omega_h \times [0,T])$, $v_h|_K \in H^1(K\times[0,T])$ and $\underline{\sigma}_h|_K \in H^1(K\times[0,T])$. The integration against discontinuous test functions w and $\underline{\xi}$ is performed locally on each triangle,

$$\begin{cases} \sum_K \int_K \rho_K \partial_t v w d\mathbf{x} = \\ \qquad \sum_K \left(\int_{\Gamma_K} \{\underline{\sigma}\mathbf{n_K}\}.[\![w]\!]d\mathbf{x} - \int_K \underline{\sigma} : \boldsymbol{\nabla} w d\mathbf{x}\right), \\ \sum_K \int_K \partial_t \underline{\sigma} : \underline{\xi} d\mathbf{x} = \\ \qquad \sum_K \left(\int_{\Gamma_K} [\![(\underline{C} : \underline{\xi})\mathbf{n_K}]\!]\{v\}d\mathbf{x} - \int_K v.\nabla.(\underline{C} : \underline{\xi})d\mathbf{x}\right), \end{cases} \quad (4)$$

with the centered fluxes formulation (i.e. the jump and mean formula chosen such that: $\{u\} = \frac{u_{K_1}+u_{K_2}}{2}$, $[\![u]\!] = u_{K_1} - u_{K_2}$).

These equations can be written as a linear system,

$$\begin{cases} \rho M_v \partial_t v_h + R_{\underline{\sigma}}\underline{\sigma}_h &= 0 \\ M_{\underline{\sigma}}\partial_t \underline{\sigma}_h + R_v v_h &= 0 \end{cases} \quad (5)$$

with M_v, $M_{\underline{\sigma}}$ block-diagonal mass matrices and R_v, $R_{\underline{\sigma}}$ stiffness matrices.

The time discretization is done with the classical leap-frog time scheme. It is an explicit scheme which is stable under a CFL condition[4] available in [4].

Time domain $[0,T]$ is divided into time steps Δt. Let v_h^n be the approximation of the velocity $v_h(t)$ at the discrete time $t = n\Delta t$ and $\underline{\sigma}_h^{n+1/2}$ the approximation of the stress tensor $\underline{\sigma}_h(t)$ at the discrete time $t = (n+\frac{1}{2})\Delta t$. Semi-discrete linear system (5) becomes

$$\begin{cases} \rho M_v \dfrac{v_h^{n+1} - v_h^n}{\Delta t} + R_{\underline{\sigma}}\underline{\sigma}_h^{n+1/2} &= 0 \\ M_{\underline{\sigma}} \dfrac{\underline{\sigma}_h^{n+3/2} - \underline{\sigma}_h^{n+1/2}}{\Delta t} + R_v v_h^{n+1} &= 0 \end{cases} \quad (6)$$

Since M_v and $M_{\underline{\sigma}}$ are block-diagonal due to DGM, this scheme is quasi-explicit.

4 VTI ABC

In order to simplify the presentation of the results, we only consider two cases, a rectangle mesh and a rhombus mesh (actually a rectangle mesh rotated by an angle $\pi/6$). We will formulate low-order ABCs on these meshes.

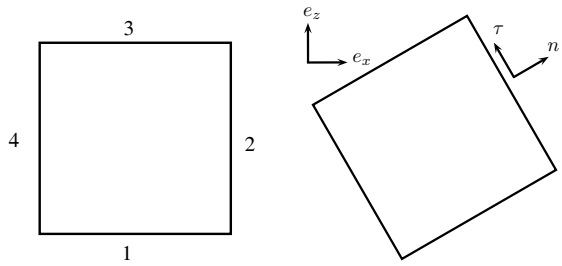

Figure 2: Rectangle and rhombus meshes

We begin with the rectangular mesh because it is easier to work on vertical and horizontal boundaries. To formulate VTI ABCs we decompose problem (1) in P-waves (resp. S-waves) by setting the velocity $V_s = 0$ (resp. $V_p = 0$). It forms two anisotropic acoustic wave equations for which we can easily construct ABCs by applying Enquist-Majda's methodology [5, 6]. For the P-waves, we obtain a condition on σ_{xx} on vertical boundaries and a condition on σ_{zz} on horizontal boundaries. For S-waves, we obtain a condition on σ_{xz} on all boundaries. These VTI ABCs are presented in Table 1, with $Cp_{max} = -\sqrt{\rho C_{11}}$, $Cp_{min} = -\sqrt{\rho C_{22}}$ and $Cs = -\sqrt{\rho C_{33}}$. In the isotropic case, we recover the low-order ABCs proposed by Tsokga [8] (called order 1/2).

Let us introduce $\mathbf{n} = (n_x, n_z)$ the normal vector exterior of each face of Γ (i.e. $\mathbf{n}$ varies depending on the face) and the associated basis $(\mathbf{n}, \boldsymbol{\tau})$, as shown in Figure 2.

[4] Courant-Friedrichs-Lewy condition is an inegality concerning time and space discretization steps. It has to be respected in order to assure numerically convergence.

Boundary	P-waves	S-waves
1	$\sigma_{zz} = -Cp_{min}v_z$	$\sigma_{xz} = -Csv_x$
2	$\sigma_{xx} = +Cp_{max}v_x$	$\sigma_{xz} = +Csv_z$
3	$\sigma_{zz} = +Cp_{min}v_z$	$\sigma_{xz} = +Csv_x$
4	$\sigma_{xx} = -Cp_{max}v_x$	$\sigma_{xz} = -Csv_z$

Table 1: VTI ABCs on the rectangle boundaries

The boundary conditions are localized on the boundary of the mesh Ω_h. In the 2D case, it concerns the edges Γ of the triangles K in contact with the mesh boundary. Thus, in the numerical scheme the boundary conditions appear in the surface integral term, i.e. in the integral on Γ. Note that the DGM formulation (4) contains two surface integral terms. One is in the first equation, reading as an integral of $\underline{\underline{\sigma}}\mathbf{n}$ and one is in the second equation, reading as an integral of v. The ABC can be included in the formulation by plugging the equation of Table 1 into one of these terms. We arbitrarily decided to consider the first one:

$$\int_\Gamma \underline{\underline{\sigma}}\mathbf{n}_\Gamma . w d\mathbf{x}. \tag{7}$$

In order to obtained ABCs for an arbitrary face of normal $\mathbf{n}$, it is useful to decompose $\underline{\underline{\sigma}}\mathbf{n}$ in the $(\mathbf{n}, \boldsymbol{\tau})$ basis:

$$\underline{\underline{\sigma}}.\mathbf{n} = \begin{pmatrix} \sigma_{nn} & \sigma_{n\tau} \\ \sigma_{\tau n} & \sigma_{\tau\tau} \end{pmatrix} . \begin{pmatrix} 1 \\ 0 \end{pmatrix} = \begin{pmatrix} \sigma_{nn} \\ \sigma_{\tau n} \end{pmatrix}.$$

So it is sufficient to consider σ_{nn} and $\sigma_{\tau n}$ to formulate an ABC available for any faces of the mesh. The formulation of Table 1 in the $(\mathbf{n}, \boldsymbol{\tau})$ basis can be rewritten as

$$\begin{cases} \sigma_{nn} &= Cp_{max}\mathbf{V}.\mathbf{n}, \text{ on boundaries } \{2,4\}, \\ \sigma_{nn} &= Cp_{min}\mathbf{V}.\mathbf{n}, \text{ on boundaries } \{1,3\}, \\ \sigma_{\tau n} &= Cs\mathbf{V}.\boldsymbol{\tau}, \text{ on boundaries } \{1,2,3,4\}. \end{cases} \tag{8}$$

Let us remark that in the VTI ABCs (8) we use Cp_{max} on the boundaries $\{2,4\}$ and Cp_{min} on the boundaries $\{1,3\}$. In order to obtain VTI ABCs on an arbitrary face, it seems natural to defined a velocity Cp_n depending on the face exterior normal direction $\mathbf{n}$. As TI media form ellipsoidal wavefronts (see Figure 1) we propose to consider

$$Cp_n = -\sqrt{Cp_{max}^2 n_x^2 + Cp_{min}^2 n_z^2}. \tag{9}$$

And we formulate the prototype VTI ABC:

$$\begin{cases} \sigma_{nn} &= Cp_n\mathbf{V}.\mathbf{n} \\ \sigma_{\tau n} &= Cs\mathbf{V}.\boldsymbol{\tau} \end{cases} \tag{10}$$

They are then incorporated in the surface integral term (7),

$$\int_\Gamma \begin{pmatrix} \sigma_{nn} \\ \sigma_{\tau n} \end{pmatrix} . \begin{pmatrix} w_n \\ w_\tau \end{pmatrix} = \int_\Gamma \begin{pmatrix} \sigma_{nn} \\ \sigma_{\tau n} \end{pmatrix} . \begin{pmatrix} w_x n_x + w_z n_z \\ -w_x n_z + w_z n_x \end{pmatrix} =$$

$$\int_\Gamma [(Cp_n\mathbf{V}.\mathbf{n}n_x - Cs\mathbf{V}.\boldsymbol{\tau}n_z)w_x + (Cp_n\mathbf{V}.\mathbf{n}n_z + Cs\mathbf{V}.\boldsymbol{\tau}n_x)w_z] \tag{11}$$

Numerical results of prototype VTI ABC

It is well-known that low-order ABCs generate spurious reflections. Our performance criterion to validate the VTI ABC formulation (10) is to not generate more reflected waves than those of the isotropic case, which will serve as reference case. Figure 3 depicts the evolution of the magnitude of v at two time steps ($t = 1$s and $t = 5$s) in an isotropic medium. It shows that the propagated wave is absorbed and the magnitude of the reflection waves is one power of ten less.

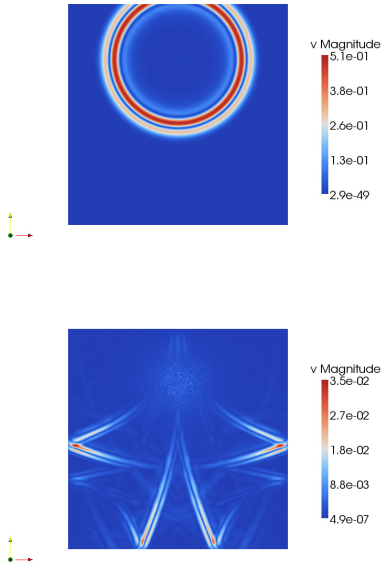

Figure 3: Isotropic reference case

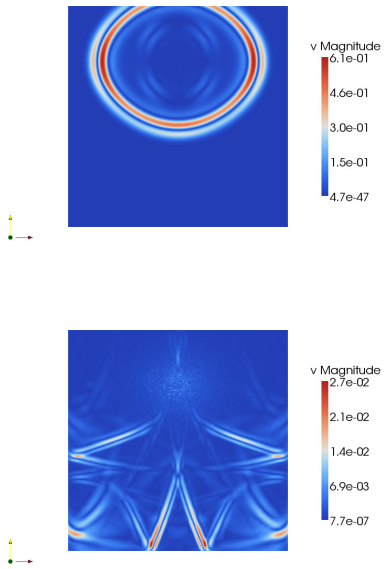

Figure 4: VTI, rectangle mesh

The prototype VTI ABC performs well in the rectangular mesh, see Figure 4. The magnitude of the reflections, which are due to the low-order ABC model is similar to the one measured in the isotropic case. The differences between Figure 3 and Figure 4, localized at the bottom corners, are due

to S-waves. Indeed a P-waves source generates S-waves in a TI medium.

On the contrary, prototype VTI ABC induces additional reflected S-waves in the rhombus mesh, polluting thus the image, see Figure 5. Actually it is important that the VTI ABC perfoms as well in the rectangle case as in the rhombus case. Indeed VTI on a rhombus mesh is equivalent to TTI on a rectangular mesh with the corresponding TTI angle.

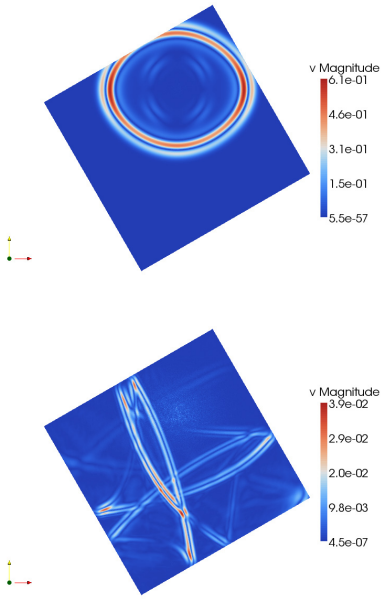

Figure 5: Prototype VTI, rhombus mesh

Therefore, we have to improve the prototype VTI ABC. To this aim, we rewrite the term (11) and we replace the coefficient Cp_n by Cp_{max} in the first part and by Cp_{min} in the second part:

$$\int_\Gamma [(Cp_{max}\mathbf{V}.\mathbf{n}n_x - Cs\mathbf{V}.\boldsymbol{\tau}n_z)w_x + (Cp_{min}\mathbf{V}.\mathbf{n}n_z + Cs\mathbf{V}.\boldsymbol{\tau}n_x)w_z] \quad (12)$$

This can be obtained from the new ABC VTI formulation:

$$\begin{cases} \sigma_{nn} &= (Cp_{max}n_x^2 + Cp_{min}n_z^2)\mathbf{V}.\mathbf{n} \\ \sigma_{\tau n} &= -((Cp_{max} - Cp_{min})n_x n_z)\mathbf{V}.\mathbf{n} + Cs\mathbf{V}.\boldsymbol{\tau} \end{cases} \quad (13)$$

Numerical results of VTI ABC

Let us remark that the new VTI ABC coincides with the prototype one for horizontal and vertical boundaries. The results are thus the same in the rectangle mesh while the new VTI ABC perfoms well now in the rhombus mesh: additional S-wave reflections have disappeared, see Figure 6.

5 TTI ABC

As explained above, TTI simulation in a rectangular mesh (which is the interesting case for geophysics), is similar to VTI simulation in a rotated mesh. Thus, to extend the above VTI ABC to TTI, we define $\mathbf{n}'$ by (see Figure 7)

$$\begin{pmatrix} n'_x \\ n'_z \end{pmatrix} = \begin{pmatrix} \cos\theta \\ \sin\theta \end{pmatrix}.$$

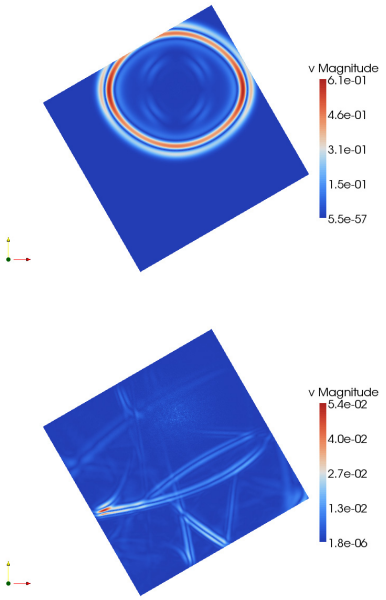

Figure 6: VTI, rhombus mesh

We underline that $\mathbf{n}'$ is independent of the boundary (contrary to $\mathbf{n}$, the face exterior normal).

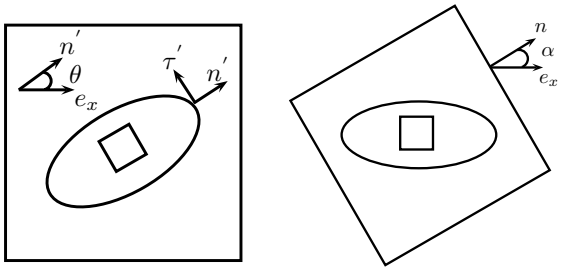

Figure 7: $(\mathbf{n}', \boldsymbol{\tau}')$ basis, θ and α angles

In the new VTI ABC (13), (n_x, n_z) are the coordinates of $\mathbf{n}$ in the $(\mathbf{n}', \boldsymbol{\tau}')$ basis, which reduces in the VTI case to $(\mathbf{e_x}, \mathbf{e_z})$. Let us introduce for TTI the vector (l_x, l_z): the coordinates of $\mathbf{n}$ in the $(\mathbf{n}', \boldsymbol{\tau}')$ basis. Using the TTI angle θ and the boundary angle α, defined in Figure 7, (l_x, l_z) reads as

$$\begin{pmatrix} l_x \\ l_z \end{pmatrix} = \begin{pmatrix} \cos(\alpha - \theta) \\ \sin(\alpha - \theta) \end{pmatrix}.$$

Thus, following the same reasoning, the TTI ABC can be formulated as:

$$\begin{cases} \sigma_{nn} &= (Cp_{max}l_x^2 + Cp_{min}l_z^2)\mathbf{V}.\mathbf{n} \\ \sigma_{\tau n} &= -((Cp_{max} - Cp_{min})l_x l_z)\mathbf{V}.\mathbf{n} + Cs\mathbf{V}.\boldsymbol{\tau} \end{cases} \quad (14)$$

We specify that the coefficients Cp_{max}, Cp_{min}, Cs of the TTI ABC come from the VTI tensor. Thereby, they do not vary with the TTI angle θ (contrary to the tensor in the TTI equation).

Numerical results of TTI ABC

The TTI ABC performs well (as well as in the VTI and the isotropic cases) in the rectangular mesh, see Figure 8. Moreover, other tests show that it gives similar results on arbitrary meshes and for any θ.

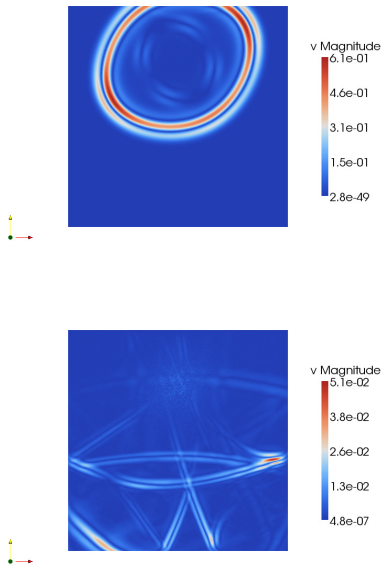

Figure 8: TTI ($\theta = \frac{\pi}{6}$), rectangle mesh

6 Conclusion

We have proposed a new Absorbing Boundary Condition for Tilted Transverse Isotropic media which can be easily included in a Discontinuous Galerkin Method formulation with few additional computational costs. As all the low-order ABCs, it generates spurious reflections, but their amplitudes are comparable to the reflections produced by low-order ABCs in isotropic media. Since low-order ABCs do not impact the accuracy of Reverse Time Migration images in isotropic media, we expect the new ABC to be efficient in a RTM framework. This should be confirmed by the numerical tests we are now performing. In a future work, we will extend the methodology in order to obtain higher (and therefore more accurate) ABCs.

Acknowledgments

The authors acknowledge the support by the INRIA-TOTAL strategic action DIP (`http://dip.inria.fr`).

References

[1] Eliane Bécache, Sandrine Fauqueux, and Patrick Joly. Stability of perfectly matched layers, group velocities and anisotropic waves. *Journal of Computational Physics*, 188(2):399–433, 2003.

[2] J.-P. Bérenger. A perfectly matched layer for the absorption of electromagnetic waves. *Journal of computational physics*, 114:185–200, 1994.

[3] J. P. Bérenger. Three-dimensional perfectly matched layer for the absorption of electromagnetic waves. *J. of Comp. Phys.*, 127:363–379, 1996.

[4] S. Delcourte, L. Fezoui, and N. Glinsky-Olivier. A high-order discontinuous galerkin method for the seismic wave propagation. *ESAIM: Proceedings*, 27:70–89, 2009. CANUM 2008.

[5] B. Engquist and A. Majda. Absorbing boundary conditions for the numerical simulation of waves. *Math. Comp.*, 31:629–651, 1977.

[6] B. Engquist and A. Majda. Radiation boundary conditions for acoustic and elastic wave calculations. *Comm. Pure Appl. Math.*, 32:314–358, 1979.

[7] L. Thomsen. Weak elastic anisotropy. *Geophysics*, 51(10):1954–1966, 1986.

[8] C. Tsogka. *Modélisation mathématique et numérique de la propagation des ondes élastiques tridimensionnelles dans des milieux fissurés*. PhD thesis, Paris IX Dauphine, 1999.

[9] I. Tsvankin. *Seismic signatures and analysis of reflection data in anisotropic media*. Elsevier, 2001.

[10] J. Virieux. P-SV wave propagation in heterogeneous media: velocity-stress finite-difference method. *Geophysics*, 51:889–901, 1986.